DRAFT VERSION MARCH 3, 2007
Preprint typeset using LaTeX style emulateapj v. 02/07/07

VELOCITY DISPERSION PROFILES OF SEVEN DWARF SPHEROIDAL GALAXIES: A UNIVERSAL PROFILE?*

MATTHEW G. WALKER[1], MARIO MATEO[1], EDWARD W. OLSZEWSKI[2], OLEG Y. GNEDIN[1], XIAO WANG[3], BODHISATTVA SEN[4], AND MICHAEL WOODROOFE[4]

Draft version March 3, 2007

ABSTRACT

We present stellar velocity dispersion profiles for seven of the Milky Way's dwarf spheroidal (dSph) satellite galaxies. We have measured 7287 line-of-sight velocities ($\pm 2-3$ km s^{-1}) for 5780 stars using high-resolution, fiber spectrographs at the Magellan and MMT telescopes. We combine these new data with previously published velocities in order to obtain the largest available kinematic samples, which include nearly 4900 probable dSph members. All the measured dSphs have stellar velocity dispersions of order 10 km s^{-1} that remain constant with distance from the dSph center, out to and in some cases beyond the radius at which the mean surface brightness falls to the background level. For a narrow range of halo masses, $2 \leq M_{vir}/(10^9 M_\odot) \leq 4$, we obtain reasonable fits to all the empirical profiles using the NFW-like density law suggested by Navarro et al. (2004). The typical dSph has $M(r < 1\text{kpc}) \sim 10^8 M_\odot$ if we integrate over only the radii sampled by the data. A non-parametric analysis yields mass estimates similar to the NFW-like profiles, lending support to the notion that the smallest galactic systems may share the same density profile.

Subject headings: galaxies: dwarf — galaxies: kinematics and dynamics — (galaxies:) Local Group — (cosmology:) dark matter — techniques: radial velocities

1. INTRODUCTION

The study of resolved stellar populations in Local Group dwarf spheroidal (dSph) galaxies has elevated dSphs from the perceived status of cosmic debris to objects of perhaps fundamental physical importance. Spanning the absolute magnitude range $-13 \leq M_V \leq -5$ (Mateo 1998; Willman et al. 2005; Belokurov et al. 2006), dSphs occupy the small extreme of the galaxy luminosity function. The Milky Way's (MW's) ~ 15 known dSph satellites have managed thus far to avoid and/or to survive interactions that consumed many of their likely siblings during hierarchical construction of the MW and M31 halos. The first speculation that dSphs might contain a dominant dark matter component was based on the velocity dispersion measured from just four stars in the Draco dSph (Aaronson 1983). Later studies (e.g., Mateo et al. 1991, 1993; Armandroff et al. 1995; Hargreaves et al. 1994, 1996) confirmed Aaronson's result, using samples of tens of stellar velocities to show that dSphs as a class have internal velocity dispersions of ~ 10 km s^{-1}, larger than can be attributed to the gravitational potential of a stellar component in virial equilibrium. Thus dSphs are the smallest stellar systems falling clearly under the dark matter paradigm.

Recent velocity measurements for up to several hundred stars per dSph (Kleyna et al. 2002, 2003, 2004; Muñoz et al. 2005, 2006; Walker et al. 2006a,b) demonstrate that dSph velocity dispersions are nearly constant with radius to the outermost data point. Anlayses that recover $M(r)$ from the Jeans Equation conclude that dSphs possess dominant and extended dark matter halos of up to $10^8 M_\odot$, except perhaps in cases where the stellar velocity distributions are highly anisotropic. Alternatively, large velocity dispersions that do not decline with radius are consistent with n-body simulations (e.g., Piatek & Pryor 1995; Read et al. 2006) of disrupted, low-mass satellites whose velocity dispersions are inflated by streaming motions of tidally stripped stars.

Here we present velocity dispersion profiles for seven dSph satellites of the Milky Way—Carina, Draco, Fornax, Leo I, Leo II, Sculptor, and Sextans. Profiles are calculated from new velocity data we have obtained using the Magellan and MMT telescopes (Walker et al. 2007a, Mateo et al. 2007). After combining with previously published results, samples range in size from 69 (Leo II) to 2010 (Fornax) member stars per dSph, for a total of 4868 probable members in the seven dSphs. With such a large data set, one can begin to compare meaningfully the kinematic properties of the local dSph population. All the measured dSphs exhibit flat velocity dispersion profiles, which we use to derive their mass profiles based on the assumption of equilibrium. Although we do not consider tidal disruption models here, Mateo et al. (2007) identify a radius beyond which the new Leo I data show a velocity gradient consistent with streaming motions (see also Sohn et al. 2006). Walker et al. (in prep.) compare the evidence for streaming in each galaxy.

2. OBSERVATIONS & DATA

Over six observing runs between 2004 March and 2006 October, we used the Michigan/MIKE Fiber System (MMFS) at the Magellan/Clay 6.5m telescope to obtain 6415 high-resolution echelle spectra of 5180 individual red giant candidates in the dSph galaxies Carina, Fornax, Sculptor and Sextans (see Walker et al. 2007a). MMFS spectra sample the Mg-triplet (MgT) region, spanning $5140-5180$ Å with effective resolution ~ 0.1 Å/pix ($R \sim 20000$). We measure both stellar velocity and the pseudo-equivalent width of the magnesium absorption feature. Comparisons of repeat measurements for more than 1000 stars indicate median measurement errors of ± 2 km s^{-1} and ± 0.06 Å, respectively.

Additionally we obtained 872 spectra from 600 red giant candidates in the northern dSphs Leo I, Leo II, and Draco using the multi-fiber Hectochelle spectrograph at the

*THIS PAPER INCLUDES DATA GATHERED WITH THE 6.5-M MAGELLAN TELESCOPES AT LAS CAMPANAS OBSERVATORY, CHILE, AND THE 6.5-M MMT TELESCOPE.

[1] Department of Astronomy, University of Michigan
[2] Steward Observatory, The University of Arizona
[3] Department of Mathematics and Statistics, University of Maryland, Baltimore County
[4] Department of Statistics, University of Michigan

MMT 6.5m telescope during two observing runs in 2005 March/April and 2006 April (see Mateo et al. 2007). Hectochelle spectra again sample the MgT region, over 5150-5300 Å, with effective resolution 0.01 Å/pix **??** ($R \sim 25000$). Repeat measurements for more than 100 stars indicate the Hectochelle velocities have errors ± 3 km s^{-1}.

To these new data we add 1788 velocities previously published for red giant candidates in the observed dSphs (Carina: Mateo et al. 1993; Muñoz et al. 2006; Draco: Armandroff et al. 1995; Kleyna et al. 2002; Fornax: Mateo et al. 1991; Walker et al. 2006a; Leo I: Mateo et al. 1998; Leo II: Vogt et al. 1995; Sextans: Hargreaves et al. 1994; Kleyna et al. 2004). We correct for any apparent zero-point offsets (see Walker et al. 2007) and use weighted mean velocities for stars in common with our MMFS/Hectochelle survey.

3. MEMBERSHIP

We evaluate the probability, P_{dsph_i}, that the i^{th} star is a dSph member using up to three bits of information—V_i, W_i (available only for MMFS samples), and elliptical radius[5] a_i. For each dSph observed with MMFS, left panels in Figure 1 display scatterplots of V and W. We assume 1) the joint distribution of velocity and magnesium strength for the members of a given dSph is a bivariate Gaussian with means $\langle V \rangle_{mem}$ and $\langle W \rangle_{mem}$, variances $\sigma^2_{V_0,mem}$ and $\sigma^2_{W_0,mem}$, and covariance $\sigma_{V_0W_0,mem} = \langle (V - \langle V \rangle)(W - \langle W \rangle) \rangle = 0$; 2) interlopers have magnesium strengths following a univariate Gaussian distribution with mean $\langle W \rangle_{non}$ and variance $\sigma^2_{W_0,non}$; and 3) interlopers have a non-Gaussian velocity distribution $p_{bes}(v)$ that we estimate from the Besancon Milky Way model (Robin et al. 2003) calculated along the line of sight to each dSph. The probability of obtaining spectroscopic data $Z_i \equiv (V_i, \sigma_{V_i}, W_i, \sigma_{W_i})$ for a member star is then[6]

$$p_{mem}(V_i, \sigma_{V_i}, W_i, \sigma_{W_i}) = \frac{\exp\left[-\frac{1}{2}\left(\frac{[V_i - \langle V \rangle_{mem}]^2}{\sigma^2_{V_0,mem} + \sigma^2_{V_i}} + \frac{[W_i - \langle W \rangle_{mem}]^2}{\sigma^2_{W_0,mem} + \sigma^2_{W_i}}\right)\right]}{2\pi\sqrt{(\sigma^2_{V_0,mem} + \sigma^2_{V_i})(\sigma^2_{W_0,mem} + \sigma^2_{W_i})}},$$

while the probability of observing Z_i for an interloper is

$$p_{non}(V_i, \sigma_{V_i}, W_i, \sigma_{W_i}) = \frac{p_{bes}(V_i) \exp\left[-\frac{1}{2}\frac{[W_i - \langle W \rangle_{non}]^2}{\sigma^2_{W_0,non} + \sigma^2_{W_i}}\right]}{\sqrt{2\pi(\sigma^2_{W_0,non} + \sigma^2_{W_i})}}.$$

Supposing $p(a_i)$ is a decreasing function that describes the *a priori* probability that a star at elliptical radius a_i is a dSph member, then given data Z_i, the i^{th} star is a dSph member with probability

$$P_{dsph_i} = \frac{p_{mem_i} p(a_i)}{p_{mem_i} p(a_i) + p_{non_i}(1 - p(a_i))},$$

and the expected likelihoood of the data set $\{Z_i\}_{i=1}^N$ is

$$\prod_{i=1}^{N} [p_{mem_i} p(a_i)]^{P_{dsph_i}} [p_{non_i}(1 - p(a_i))]^{1 - P_{dsph_i}}. \quad (1)$$

[5] A star's "elliptical radius" is the semi-major axis of the isophotal ellipse that passes through the star's position. Here we make the approximation that a dSph's isophotal ellipses all have common ellipticity and orientation, the values of which we adopt from Irwin & Hatzidimitriou (1995).

[6] For stars that lack an acceptable measurement of magnesium strength (including stars in the previously published samples, as well as our new Hectochelle samples), we set $\sigma_{W_i} = \infty$.

TABLE 1
SUMMARY OF DSPH VELOCITY SAMPLES AND MASS ESTIMATES

Gal.	N_{new}; N_{tot}; N_{dsph}	$M(R_{max})$ ($10^8 M_\odot$)	M(750pc) ($10^8 M_\odot$)	L_V[a] ($10^6 L_{V_\odot}$)	M/L_V ($[M/L_V]_\odot$)
Car	1312; 2136; 761	1.0[b]; 1.0[c]	0.43[b]; 0.45[c]	0.43	300[b]; 280[c]
Dra	286; 442; 374	1.3; 1.9	1.3; 1.8	0.26	890; 1200
For	1924; 2085; 2010	1.9; 3.9	0.64; 0.45	15.5	14; 27
LeoI	257; 273; 212	0.80; 1.1	0.57; 0.68	4.79	21; 28
LeoII	57; 88; 69	0.68; ···	0.68; ···	0.58	183; ···
Scl	1089; 1089; 986	1.1; 1.5	0.62; 0.95	2.15	56; 70
Sex	855; 943; 456	0.66; 1.0	0.27; 0.34	0.50	130; 190

[a] ref: Mateo 1998
[b] from N04 profile
[c] from non-parametric estimate

We use an iterative expectation-maximization (EM) algorithm (Sen et al. 2007) to estimate the unknown parameters in (1), which include the probabilities P_{dsph_i} and the Gaussian means and variances. The details of our implentation (Walker et al. in prep) differ from those outlined in Sen et al. (2007) in that we now consider magnesium absorption and we estimate the decreasing function $p(a_i)$ via isotonic regression. Marker colors in Figure 1 indicate the resulting estimate $\hat{P}_{dsph_i}$ for each star. Black markers identify the most likely interlopers ($\hat{P}_{dsph_i} < 0.01$). For the remaining stars, bluer markers indicate larger $\hat{P}_{dsph_i}$ (see caption to Figure 1). For subsequent analysis we retain all data points and weight each by $\hat{P}_{dsph_i}$.

Right-hand panels of Figure 1 plot line-of-sight velocity as a function of angular distance from the dSph center. The interloper velocity distributions obtained from the Besançon models are normalized according to the final membership ratios and overplotted in red in subpanels that indicate the (logarithm of the) overall velocity distribution. For dSphs observed with a high degree of contamination (Carina, Sextans), we find excellent agreement between the predicted and observed velocity distributions of foreground stars. Table 1 lists for each dSph the numbers of newly observed stars, total stars after combining with published data, and member stars $N_{dsph} = \sum_{i=1}^{N_{tot}} P_{dsph_i}$.

4. VELOCITY DISPERSION PROFILES

We estimate line-of-sight velocity dispersion profiles by dividing each sample into $\sim \sqrt{N_{dsph}}$ bins according to projected distance from the dSph center. For a given sample we define bins (circular annuli) such that each contains approximately equal numbers of dSph members. Thus, the number of stars (including interlopers) in each bin may vary but for all bins, $\sum_{i=1}^{N_{bin}} \hat{P}_{dsph_i} \sim \sqrt{N_{dsph}}$. We use a Gaussian maximum-likelihood method (essentially that of Walker et al. 2006a, but updated to weight data according to $\hat{P}_{dsph_i}$) to estimate the velocity dispersion within each bin. Figure 2 displays the resulting velocity dispersion profiles, which generally are consistent with flatness to the outermost data point.

Dashed lines plotted over the velocity dispersion profiles are single-component King models (King 1962, 1966) conventionally used to characterize dSph surface brightness profiles. The adopted King models are those fit by Irwin & Hatzidimitriou (1995)(IH95) and normalized to match the central velocity dispersion. Their systematic failure to predict flat profiles removes any lingering doubt that (Newtonian) mass-follows-light, equilibrium models provide a poor description of dSph kinematics.

Solid lines in Figure 2 are fit (by eye) under the assumption

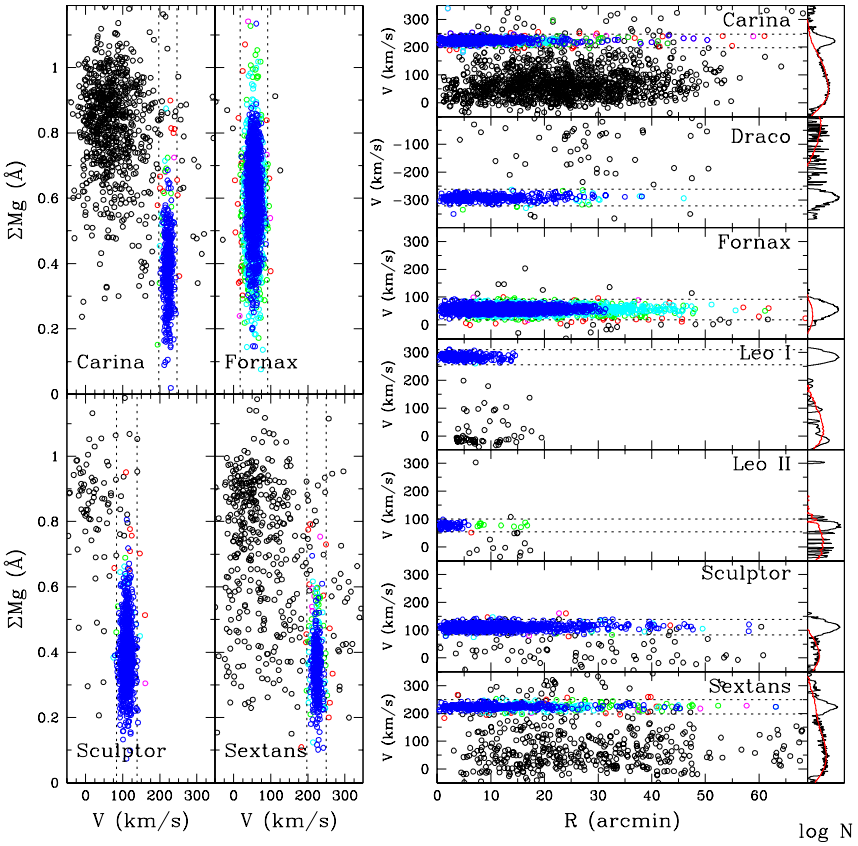

FIG. 1.— *Left:* Mg pseudo-equivalent width vs. velocity for dSph samples obtained with Magellan/MMFS. *Right:* Velocity vs. angular distance from the dSph center, including previously published velocities. The extended ($70' \leq R \leq 130'$) Carina data of Muñoz et al. (2006) fall outside the plotted region but are included in our analysis. Subpanels indicate the logarithm of the velocity distribution; red lines indicate predicted interloper distributions. In all panels, marker color indicates the probability that the star is a dSph member (Section 3). Black (red; magenta; green; cyan; blue) markers signify $P_{dsph} < 0.01$ ($P_{dsph} > 0.01; > 0.50; > 0.68; > 0.95; > 0.99$). Pairs of dotted lines enclose stars that would pass conventional membership tests based on a 3σ velocity threshold.

that the stellar component of each dSph is embedded within a dark matter halo with Sersic index $n = 3$ and concentration $c = 10$. Such halos are described by the fitting formula of Navarro et al. (2004)(N04), who find that this formula deviates from the NFW profile (Navarro et al. 1996, 1997) by less than $\sim 10\%$ and describes more faithfully the shallower (than NFW) inner density slope they obtain in recent simulations of cold dark matter. We find that the N04 fitting formula is consistent with the dSph velocity data for a surprisingly narrow range of input parameters. Assuming the stellar density of each dSph falls exponentially with scale lengths measured by IH95, we obtain reasonable fits to all the observed velocity dispersion profiles by allowing the halo mass to vary only over the narrow range $2 \leq M_{vir}/(10^9 \mathrm{M}_\odot) \leq 4$. In all cases except Leo II we assume constant, tangential anisotropy with $\beta = -0.3$; for Leo II we require $\beta = +0.3$ to fit the data under the stated assumptions.

Solid curves in the right-hand panels of Figure 2 show deprojected mass profiles corresponding to the N04 halos. For comparison, dotted curves depict mass estimates obtained using the non-parametric technique of Wang et al. (2005), which assumes only the spherical form of the Jeans Equation with $\beta = 0$ (the Leo II sample contains too few stars to produce a reliable non-parametric mass estimate). We find striking similarity between the N04 and non-parametric mass profiles for Carina, Draco, Sculptor and Sextans. Table 1 identifies $M(R_{max})$, the mass enclosed within the outermost profile point, and M(750pc), the mass enclosed within the largest radius common to all empirical profiles. Without exception, the N04 and non-parametric estimates of $M(R_{max})$ for the same dSph agree to within a factor of less than two. Considering only radii common to all samples, M(750pc) varies among the seven dSphs by a factor of less than two. The last column in Table 1 gives the enclosed mass-to-light ratio (M/L) at R_{max}. The M/L for every dSph indicates a significant dark matter component, with $14 \leq \mathrm{M/L}_V \leq 1200$. While this result is trivial for the N04 profiles, in which dark matter is assumed, the non-parametric profiles could have shown otherwise. As previous authors have noted (Mateo 1998), the dependence of $\mathrm{M/L}_V$ on absolute magnitude is monotonic. Thus the wide range of $\mathrm{M/L}_V$ appears to reflect the range of L_V, and our results are, in this simple analysis, consistent with a "universal" dSph mass profile.

5. DISCUSSION

In deriving the mass estimates above we do not consider several factors—variable anisotropy, kinematic substructure and, perhaps most importantly, the effects of external tides—that complicate a more thorough analysis of dSph kinematics. We note also that the presented profiles do not address a recent controversy concerning whether velocity dispersion drops sharply at large radius in Draco and Ursa Minor (Wilkinson et al. 2004; Muñoz et al. 2005)—neither our MMT data nor the published data reach the Draco radius in

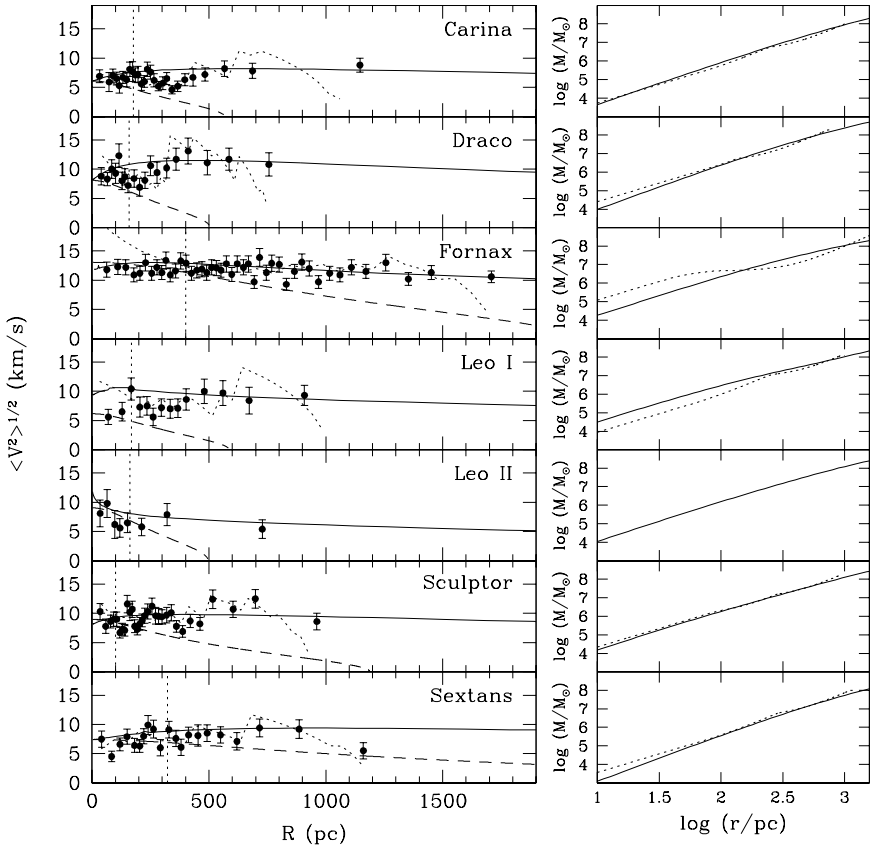

FIG. 2.— *Left:* Projected velocity dispersion profiles for seven of the Milky Way's dSph satellites. Overplotted are profiles corresponding to mass-follows light (King 1962) models (dashed lines), profiles derived from the fitting formula of Navarro et al. (2004) (solid lines), and estimates from the non-parametric technique of Wang et al. (2005). Vertical, lines indicate luminous core radii (IH95). Distance moduli are adopted from Mateo (1998) *Right:* Deprojected mass profiles corresponding to the N04 profiles (solid lines) and non-parametric estimates of Wang et al. (2005) (dotted lines).

question ($R > 1$ kpc). Regarding tides, it is well-known from N-body simulations (Oh et al. 1995; Piatek & Pryor 1995; Read et al. 2006) that tidal forces exerted by the Milky Way on its dSph satellites can inflate stellar velocity dispersions and resulting mass estimates well above equilibrium values. The masses estimated above assume for simplicity that tides are dynamically insignificant, but we acknowledge a growing body of kinematic evidence that some systems are tidally perturbed, at least in their outer regions (Muñoz et al. 2006; Sohn et al. 2006, Mateo et al. 2007). A proper consideration of tides will almost certainly reduce the derived M/L; however, even in these few well-studied cases, tides do not obviate the inference that dSphs require a significant dark matter component. In a forthcoming paper we test for kinematic evidence of tidal effects in each of our samples.

We thank the excellent staff at both the Las Campanas Observatory and the MMT Observatory. This work is supported by NSF Grants AST 05-07453, AST 02-06081, and AST 94-13847.

REFERENCES

Aaronson, M. 1983, ApJ, 266, L11
Armandroff, T. E., Olszewski, E. W., & Pryor, C. 1995, AJ, 110, 2131
Belokurov, V., Zucker, D. B., Evans, N. W., Kleyna, J. T., Koposov, S., Hodgkin, S. T., Irwin, M. J., Gilmore, G., Wilkinson, M. I., Fellhauer, M., Bramich, D. M., Hewett, P. C., Vidrih, S., De Jong, J. T. A., Smith, J. A., Rix, H. ., Bell, E. F., Wyse, R. F. G., Newberg, H. J., Mayeur, P. A., Yanny, B., Rockosi, C. M., Gnedin, O. Y., Schneider, D. P., Beers, T. C., Barentine, J. C., Brewington, H., Brinkmann, J., Harvanek, M., Kleinman, S. J., Krzesinski, J., Long, D., Nitta, A., & Snedden, S. A. 2006, ArXiv Astrophysics e-prints
Hargreaves, J. C., Gilmore, G., Irwin, M. J., & Carter, D. 1994, MNRAS, 271, 693
—. 1996, MNRAS, 282, 305
Irwin, M., & Hatzidimitriou, D. 1995, MNRAS, 277, 1354
King, I. 1962, AJ, 67, 471
King, I. R. 1966, AJ, 71, 64
Kleyna, J., Wilkinson, M. I., Evans, N. W., Gilmore, G., & Frayn, C. 2002, MNRAS, 330, 792
Kleyna, J. T., Wilkinson, M. I., Evans, N. W., & Gilmore, G. 2004, MNRAS, 354, L66
Kleyna, J. T., Wilkinson, M. I., Gilmore, G., & Evans, N. W. 2003, ApJ, 588, L21
Mateo, M., Olszewski, E., Welch, D. L., Fischer, P., & Kunkel, W. 1991, AJ, 102, 914
Mateo, M., Olszewski, E. W., Pryor, C., Welch, D. L., & Fischer, P. 1993, AJ, 105, 510
Mateo, M., Olszewski, E. W., Vogt, S. S., & Keane, M. J. 1998, AJ, 116, 2315
Mateo, M. L. 1998, ARA&A, 36, 435
Muñoz, R. R., Frinchaboy, P. M., Majewski, S. R., Kuhn, J. R., Chou, M.-Y., Palma, C., Sohn, S. T., Patterson, R. J., & Siegel, M. H. 2005, ApJ, 631, L137
Muñoz, R. R., Majewski, S. R., Zaggia, S., Kunkel, W. E., Frinchaboy, P. M., Nidever, D. L., Crnojevic, D., Patterson, R. J., Crane, J. D., Johnston, K. V., Sohn, S. T., Bernstein, R., & Shectman, S. 2006, ApJ, 649, 201
Navarro, J. F., Frenk, C. S., & White, S. D. M. 1996, ApJ, 462, 563
—. 1997, ApJ, 490, 493

Navarro, J. F., Hayashi, E., Power, C., Jenkins, A. R., Frenk, C. S., White, S. D. M., Springel, V., Stadel, J., & Quinn, T. R. 2004, MNRAS, 349, 1039
Oh, K. S., Lin, D. N. C., & Aarseth, S. J. 1995, ApJ, 442, 142
Piatek, S., & Pryor, C. 1995, AJ, 109, 1071
Read, J. I., Wilkinson, M. I., Evans, N. W., Gilmore, G., & Kleyna, J. T. 2006, MNRAS, 366, 429
Robin, A. C., Reylé, C., Derrière, S., & Picaud, S. 2003, A&A, 409, 523
Sohn, S. T., Majewski, S. R., Munoz, R. R., Kunkel, W. E., Johnston, K. V., Ostheimer, J. C., Guhathakurta, P., Patterson, R. J., Siegel, M. H., & Cooper, M. C. 2006, ArXiv Astrophysics e-prints
Tolstoy, E., Irwin, M. J., Helmi, A., Battaglia, G., Jablonka, P., Hill, V., Venn, K. A., Shetrone, M. D., Letarte, B., Cole, A. A., Primas, F., Francois, P., Arimoto, N., Sadakane, K., Kaufer, A., Szeifert, T., & Abel, T. 2004, ApJ, 617, L119
Vogt, S. S., Mateo, M., Olszewski, E. W., & Keane, M. J. 1995, AJ, 109, 151
Walker, M. G., Mateo, M., Olszewski, E. W., Bernstein, R., Wang, X., & Woodroofe, M. 2006a, AJ, 131, 2114
Walker, M. G., Mateo, M., Olszewski, E. W., Pal, J. K., Sen, B., & Woodroofe, M. 2006b, ApJ, 642, L41
Wang, X., Woodroofe, M., Walker, M. G., Mateo, M., & Olszewski, E. 2005, ApJ, 626, 145
Wilkinson, M. I., Kleyna, J. T., Evans, N. W., Gilmore, G. F., Irwin, M. J., & Grebel, E. K. 2004, ApJ, 611, L21
Willman, B., Dalcanton, J. J., Martinez-Delgado, D., West, A. A., Blanton, M. R., Hogg, D. W., Barentine, J. C., Brewington, H. J., Harvanek, M., Kleinman, S. J., Krzesinski, J., Long, D., Neilsen, Jr., E. H., Nitta, A., & Snedden, S. A. 2005, ApJ, 626, L85